Generic Modeling and Control Framework for Power Systems Dominated by Power Converters Connected through a Passive T&D Grid

Qing-Chang Zhong, *Fellow, IEEE,* and Márcio Stefanello, *Member, IEEE*

***Abstract*—In this paper, a compact mathematical model having an elegant structure, together with a generic control framework, are proposed for generic power systems dominated by power converters that are interconnected through a passive transmission and distribution (T&D) grid, by adopting the port-Hamiltonian (pH) systems theory and the fundamental circuit theory. The models of generic T&D lines are developed and then the model of a generic T&D grid is established. With the proposed control framework, the controlled converters are proven to be passive and Input-to-State Stable (ISS). The compact mathematical model is scalable and can be applied to power systems with multiple power electronic converters with generic passive controllers, passive local loads, and different types of passive T&D lines connected in a meshed configuration without self-loops, so it is very generic. Moreover, the resulting power system is proven to be ISS as well. The analysis is carried out without assumptions on constant frequency/voltage, constant loads, and/or lossless networks, except the need of passivity for all parts involved, and without using the Clarke/Park transformations or the graph theory. To simplify the presentation, three-phase balanced systems are adopted but the results can be easily adapted for single-phase or unbalanced three-phase systems.**

***Index Terms*—Power electronic converters dominated power systems, passivity, Input-to-State Stable (ISS), port-Hamiltonian (pH) systems, Synchronized and Democratized (SYNDEM) grid architecture.**

I. Introduction

Power systems are going through a paradigm change. The penetration of the energy processed by power electronic converters is increasing, mainly due to the widespread use of distributed energy resources [1], [2], [3]. Whether operated independently or collectively in a power system, there is an increasing need for power electronic converters to take part in the regulation of system voltage and frequency. In particular, operating a power converter as a virtual synchronous machine (VSM) [4], [1] has solved the compatibility problem of distributed energy resources with the current power systems, which are dominated by synchronous machines. Moreover, the power electronic rectifiers in the majority of loads can be operated as VSM as well. This makes it possible to unify and harmonize the integration and interaction of heterogeneous power system players with the grid, which results in a homogenized architecture, referred to as the Synchronized and Democratized (SYNDEM) grid architecture [1], as shown in Figure 1. Because of the SYNDEM grid architecture is homogenized, it is now possible to solve some challenging open problems in power systems.

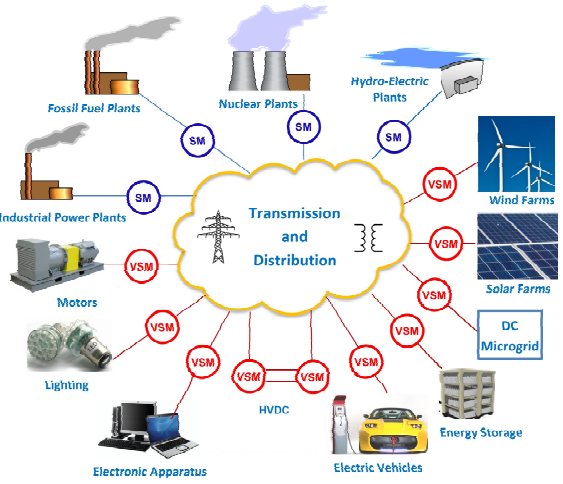

Figure 1. The Synchronized and Democratized (SYNDEM) grid architecture that unifies the integration and interaction of synchronous machines (SM), distributed energy resources, and the majority of loads through operating power electronic converters as virtual synchronous machines (VSM) [1].

One challenging problem is the modeling of power systems with high penetration of power converters interconnected by transmission and distribution (T&D) lines and arranged in different topologies. A framework is proposed in [5] to model power systems with resistive-inductive (RL) T&D lines as a port-Hamiltonian (pH) system on a graph with edges corresponding to components of power systems, nodes corresponding to buses, and the graph incidence matrix to capture the structure of the system as the interconnection constraints. However, because of the heterogeneous nature of the components and the complexity of power systems, it is still an open problem to model large-scale power systems that preserves the structure and dynamics while maintaining the feasibility for analysis. Another interesting approach is presented in [6]. Generators are not accounted in the modeling process, but the the controller is designed to ensure synchronization under proper power setpoints that depends on the line parameters of an RL T&D in a meshed configuration. The modeling and

Q.-C. Zhong is with the Department of Electrical and Computer Engineering, Illinois Institute of Technology, Chicago, IL 60616, USA, and Syndem LLC, USA. Email: zhongqc@iccc.org.

M. Stefanello is with the Fundação Universidade Federal do Pampa at Alegrete, RS, 97546-550, BR. Email: marciost@iccc.org.

This work was partially supported by NSF, USA, under award #1810105 and Foundation for Research Support of the State of Rio Grande do Sul (FAPERGS), BR, under grant number 21/2551-0002158-6, CfP PqG 2021.

control with Kuramoto models have also been proposed; see, e.g. [7] and [8]. It is proved that the power sharing is achieved only if the droop coefficients are selected proportionally. It is important to mention that the results hold without assumptions on identical line characteristics or voltage magnitudes. Among these modeling approaches, the use of pH systems allows the modeling of complex systems via power ports to interact with the environment, which is consistent with multi-converter power systems, where the nodes, i.e., the power converters, are interfaced with the grid via channels described by voltages and currents at their terminals.

Another challenge is stability of power systems [6], [9], [10]. As is well known, there exists coupling between frequency and voltage channels, e.g. in the controller of power converters. Also, there are nonlinearities in the calculation of real power and reactive power. Furthermore, there are nonlinear loads. These features impair the assessment of stability via classical tools, such as small-signal analysis and linearization, despite the clarifying conclusions that can be obtained by applying these tools; see, e.g., [11]. Thus, the use of mathematical tools for nonlinear systems has become a necessity to assess stability, actually, not only the stability itself, but also the model of the overall system. Notably, Lyapunov-based frameworks have been widely used; see, e.g., [12], [13]. Another powerful tool is the pH systems theory [14], [15], [5], [16], [17]. It is a promising tool to address the problems of modeling, analysis and design of controllers for passivization and stabilization of nonlinear systems. It has been applied to different systems, including power systems, e.g., in[10], [18], [9]. The authors recently adopted this theory to introduce a generic control framework in [19] along the line of operating a power converter as a VSM to render a power converter passive with the only assumption of the loads being passive. However, no stability analysis was carried out there.

This paper addresses the problems of modeling and control of power systems dominated by DC/AC power converters connected through a generic passive T&D grid in a meshed configuration, by adopting the pH systems theory [20], [16]. The T&D lines, which can be of different types, such as T-type, π-type, and RL-type, are modeled in the pH format and then a pH model for the overall power grid is obtained by stacking the models up, only based on the Kirchhoff's Current & Voltage Laws (KCL & KVL) without using the graph theory or the Clarke/Park transformations. It is shown that the power grid preserves the same basic properties regardless of adding, subtracting or rearranging the T&D lines. The model of the overall power grid has power ports formed by voltages and currents, facilitating the integration of every single power converter into the power grid. Then, a generic framework with a passive controller in the pH format is proposed to control the power converters. As a result, each controlled power converter is passive and Input-to-State Stable (in short, ISS). Moreover, the model of the overall power system with controlled converters is derived and described in a compact pH format. Furthermore, the overall power system is proven to be passive and also ISS. It is important to highlight that there is no need to assume the dominance of the resistive part over the reactive part, or vice-versa, for a T&D line. The modeling and control framework is scalable in the sense that it can easily accommodate multiple power converters and multiple T&D lines, without losing the capability of capturing the dynamics. It is expected that this generic framework would pave the way to prove the (asymptotic) stability of power systems dominated by power converters connected through a passive T&D grid because an ISS system is globally asymptotically stable with zero input and is bounded-input-bounded-output stable. This problem is currently under investigation.

It is expected that this generic framework would pave the way to prove the (asymptotic) stability of power systems dominated by power converters connected through a passive T&D grid because an ISS system is globally asymptotically stable with zero input and is bounded-input-bounded-output stable. This problem is currently under investigation.

The rest of the paper is organized as follows. In Section II, some preliminaries are given. In Section III, the model for passive T&D lines is developed at first and then the model for a generic power grid with passive T&D lines in a meshed configuration is developed. In Section IV, a generic control framework is proposed. Then, in Section V, the model of the overall power system with multiple power converters is developed and its ISS is proven. In Section VI, simulation results are presented and, finally in Section VII, conclusions are made.

II. Preliminaries

The symbol I stands for the 3×3 identity matrix. The notation $\mathcal{S} = \{1, \ldots, N_S\}$ denotes the set of N_S elements and $M \in \{A, B, \ldots\}^{N_R \times N_C}$ stands for the matrix $M \in \mathbb{R}^{N_R \times N_C}$ with entries A's, B's,.... The length of the vector $z_0 = \begin{bmatrix} z_{01} & \ldots & z_{0n_0} \end{bmatrix}^T$ is captured by its Euclidean norm $\|z_0\|_2 = \sqrt{z_{01}^2 + \ldots + z_{0n_0}^2}$. In the sequel, the dependence of some quantities on state variables may be omitted for convenience.

The input-state-output pH system is given by

$$\begin{aligned} \dot{z} &= \left[J_0(z) - R_0(z)\right] \frac{\partial H_0(z)}{\partial z} + G_0^T(z) u_0 \\ y_0 &= G_0(z) \frac{\partial H_0(z)}{\partial z}, \end{aligned} \tag{1}$$

with the state $z \in \mathbb{R}^{n_0 \times 1}$, input/output pair u_0, $y_0 \in \mathbb{R}^{m_0 \times 1}$, smooth matrices $J_0(z) = -J_0^T(z) \in \mathbb{R}^{n_0 \times n_0}$ and $R_0(z) = R_0^T(z) \geq 0 \in \mathbb{R}^{n_0 \times n_0}$, bounded matrix $G_0(z) \in \mathbb{R}^{n_0 \times m_0}$, and the energy function $H_0(z) : \mathbb{R}^{n_0} \to \mathbb{R}$, which is commonly referred to as the Hamiltonian. If H_0 is bounded from below, then the system (1) is passive in the sense that it cannot store more energy than supplied to it from the outside via the *supply rate* $u_0^T y_0$, with the difference dissipated via $R_0(z) \geq 0$, because

$$\dot{H}_0(z) = -\frac{\partial H_0^T(z)}{\partial z} R_0(z) \frac{\partial H_0(z)}{\partial z} + u_0^T y_0 \leq u_0^T y_0.$$

The input output pair (u_0, y_0) defines the power port of the pH model (1) because $u_0^T y_0$ has the unit of power.

Lemma 1. *The system (1) having the Hamiltonian $H_0(z) = \frac{1}{2} z^T M_0 z$, with the constant matrix $M_0 = M_0^T > 0 \in \mathbb{R}^{n_0 \times n_0}$,*

is ISS for any bounded input u_0 if $R_0 > 0$. In other words, there exists functions $\beta \in \mathcal{KL}$ and $\gamma \in \mathcal{K}$ such that

$$\|z(t)\|_2 \leq \beta\left(\|z(0)\|_2, t\right) + \gamma\left(\sup_{0\leq\tau\leq t}\|u_0(\tau)\|_2\right), \ \forall t \geq 0 \tag{2}$$

for all initial values $z(0)$ and all admissible inputs u_0.

Proof: This can be proven by following the reasoning in [21, the first part of the proof for Proposition 1].

Since $H_0(z) = \frac{1}{2}z^T M_0 z$ with $M_0 = M_0^T > 0$, there is $\frac{\partial H_0(z)}{\partial z} = M_0 z$. From the state equation of (1), there is

$$M_0\dot{z} = \left(M_0 J_0 M_0 - M_0 R_0 M_0\right) z + M_0 G_0^T u_0. \tag{3}$$

Moreover, the Hamiltonian $H_0 = \frac{1}{2}z^T M_0 z$ indicates that

$$\frac{1}{2}\lambda_{min}(M_0)\|z\|_2^2 \leq \quad H_0(z) \quad \leq \frac{1}{2}\lambda_{max}(M_0)\|z\|_2^2, \tag{4}$$

where $\lambda_{min}(M)$ and $\lambda_{max}(M)$ indicate the smallest and largest eigenvalues of M, respectively, and

$$\begin{aligned}\dot{H}_0 &= \left(\frac{\partial H_0(z)}{\partial z}\right)^T \dot{z} = z^T M_0 \dot{z} \\ &= z^T\left[\left(M_0 J_0 M_0 - M_0 R_0 M_0\right) z + M_0 G_0^T u_0\right] \\ &= -z^T M_0 R_0 M_0 z + z^T M_0 G_0^T u_0\end{aligned} \tag{5}$$

because $M_0 J_0 M_0$ is skew-symmetric. According to the properties of norms, there is

$$\dot{H}_0 \leq -\lambda_{min}(M_0 R_0 M_0)\|z\|_2^2 + c\|z\|_2\|u_0\|_2, \tag{6}$$

where $c > 0$ stands for the maximum absolute value among the entries of $M_0 G_0^T$. Hence, there exists $0 < \theta < 1$ such that

$$\begin{aligned}\dot{H}_0 \leq\ & -(1-\theta)\lambda_{min}(M_0 R_0 M_0)\|z\|_2^2 \\ & -\theta\lambda_{min}(M_0 R_0 M_0)\|z\|_2^2 + c\|z\|_2\|u_0\|_2 \\ \leq\ & -(1-\theta)\lambda_{min}(M_0 R_0 M_0)\|z\|_2^2, \\ & \forall\ \|z\|_2 \geq \frac{c}{\theta\lambda_{min}(M_0 R_0 M_0)}\|u_0\|_2.\end{aligned}$$

This, together with (4), imply that the system (1) having $R_0 > 0$ and the Hamiltonian $H_0(z) = \frac{1}{2}z^T M_0 z$, with $M_0 = M_0^T > 0 \in \mathbb{R}^{n_0\times n_0}$ being a constant matrix, is ISS with

$$\gamma = \sqrt{\frac{\lambda_{max}(M_0)}{\lambda_{min}(M_0)}}\frac{c}{\theta\lambda_{min}(M_0 R_0 M_0)}\sup_{0\leq\tau\leq t}\|u_0(\tau)\|_2, \tag{7}$$

according to [21]. This concludes the proof. ∎

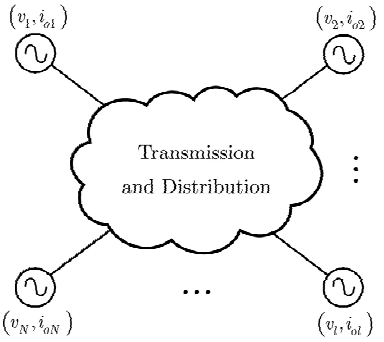

Figure 2. A generic power system $\hat{\Sigma}$ with N nodes.

III. Modeling of Power Grids

This section is devoted to the modeling of a generic power grid $\hat{\Sigma}$ shown in Figure 2 with N nodes, which can be power converters or generators. It is assumed to be a three-phase system but the development below can be applied to single-phase systems as well after some minor changes. The system is assumed to be balanced to facilitate the presentation in the sequel, but it can be easily modified to cover unbalanced systems as well.

Denote the set of nodes as $\mathcal{N} = \{1, \ldots, N\}$. Without loss of generality, assume that each converter or generator is described by a pair of output voltage and input current as (v_l, i_{ol}), $l \in \mathcal{N}$. The set $\mathcal{E} \in (\mathcal{N}\times\mathcal{N}) \setminus \cup_{l\in\mathcal{N}}(l, l)$ is related to the T&D grid, with a total number of M T&D lines arranged in a meshed configuration without self-loops. This assumption is reasonable because, in practice, no T&D lines exist to link a node with itself.

A. Modeling of T&D Lines

T&D lines can be regarded as dynamic systems that interact with the environment through two ports, as illustrated in Figure 3. Each port is connected to a node represented by its respective index j or k, with $j, k \in \mathcal{N} \setminus \{j = k\}$. The values $v_j, v_k \in \mathbb{R}^3$ stand for the voltages at their corresponding nodes, i.e., at the ends of a T&D line. The currents $i_{jk}, i_{kj} \in \mathbb{R}^3$ represent the currents flowing into the T&D line from the node j to k, and from the node k to j, respectively. Note that, in general, there is no need to assume or require $i_{jk} = i_{kj}$.

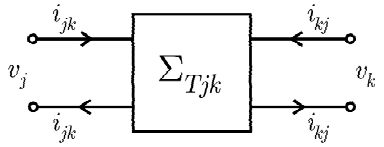

Figure 3. Two-port representation of a passive T&D line between the nodes j and k.

It is reasonable to assume that all T&D lines are passive, as this is the case in practice. Also, it is usually assumed that there is a large resistor, often in the range of Mega-Ohms, in parallel with a capacitor. This is followed in this paper, without explicitly showing the resistor in the figures to simplify the presentation, and the resistor is denoted as r_∞.With these assumptions, the T&D line shown in Figure 3 can be modeled with the pH model as

$$\Sigma_{Tjk}: \begin{cases} \dot{x}_{Tjk} = \left(J_{Tjk} - R_{Tjk}\right)\dfrac{\partial H_{Tjk}}{\partial x_{Tjk}} + \begin{bmatrix} G_{jk}^T & G_{kj}^T \end{bmatrix}\begin{bmatrix} v_j \\ v_k \end{bmatrix} \\ \begin{bmatrix} i_{jk} \\ i_{kj} \end{bmatrix} = \begin{bmatrix} G_{jk} \\ G_{kj} \end{bmatrix}\dfrac{\partial H_{Tjk}}{\partial x_{Tjk}}, \end{cases} \tag{8}$$

with appropriate matrices $G_{jk}, G_{kj} \in \{0, I\}^{3\times 3n}$, $J_{Tjk} = -J_{Tjk}^T$, $R_{Tjk} = R_{Tjk}^T > 0$, the Hamiltonian $H_{Tjk}(x_{Tjk}) : \mathbb{R}^{3n} \to [0, \infty)$, the input voltage $\begin{bmatrix} v_j \\ v_k \end{bmatrix}$ and the output

current $\begin{bmatrix} i_{jk} \\ i_{kj} \end{bmatrix}$. The value of n depends on the type of the T&D line considered and reflects the number of the states of the T&D line.

Several typical T&D lines, including the resistive-inductive (RL) lines, the T-type T&D lines and the π-type T&D lines, are described below as examples.

1) Modeling of RL T&D Lines: An RL T&D line is illustrated as shown in Figure 4.

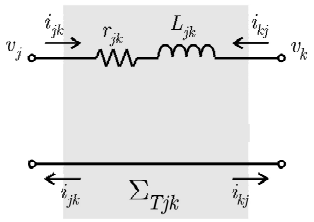

Figure 4. An RL T&D line between the nodes j and k

According to the KVL, there is

$$L_{jk}\frac{di_{jk}}{dt} = -r_{jk}i_{jk} + v_j - v_k \quad . \tag{9}$$

By selecting the state vector of the T&D line as

$$x_{Tjk} = \left[L_{jk}i_{jk}^T\right]^T \tag{10}$$

and the Hamiltonian function as

$$H_{Tjk} = \frac{1}{2}L_{jk}i_{jk}^T i_{jk}, \tag{11}$$

the RL T&D line (9) can be expressed in the generic pH format (8) with $\frac{\partial H_{Tjk}}{\partial x_{Tjk}} = \left[i_{jk}^T\right]^T$, $R_{Tjk} = \text{diag}\left(r_{jk}I\right) > 0$, $G_{jk} = I$, $G_{kj} = -I$ and $J_{Tjk} = 0$.

2) Modeling of T-type T&D Lines: A T-type T&D line is illustrated as shown in Figure 5.

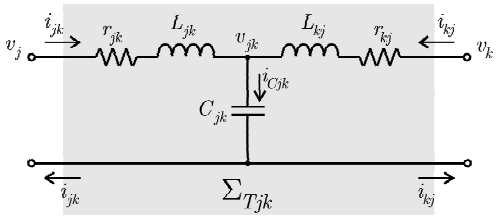

Figure 5. A T-type T&D line between the nodes j and k

According to the KCL/KVL, there are

$$\begin{aligned} L_{jk}\frac{di_{jk}}{dt} &= -r_{jk}i_{jk} - v_{jk} + v_j \\ C_{jk}\frac{dv_{jk}}{dt} &= i_{jk} + i_{kj} - \frac{1}{r_\infty}v_{jk} \\ L_{kj}\frac{di_{kj}}{dt} &= -v_{jk} - r_{kj}i_{kj} + v_k, \end{aligned} \tag{12}$$

where v_{jk} stands for the capacitor voltages at the center and r_∞ denotes the large resistor in parallel with the capacitor (not shown in the figure). By selecting the state vector of the T&D line as

$$x_{Tjk} = \begin{bmatrix} L_{jk}i_{jk}^T & C_{jk}v_{jk}^T & L_{kj}i_{kj}^T \end{bmatrix}^T \tag{13}$$

and the Hamiltonian function as

$$H_{Tjk} = \frac{1}{2}L_{jk}i_{jk}^T i_{jk} + \frac{1}{2}C_{jk}v_{jk}^T v_{jk} + \frac{1}{2}L_{kj}i_{kj}^T i_{kj}, \tag{14}$$

the T-type T&D line (12) shown in Figure 5 can be expressed in the generic pH format (8) with $\frac{\partial H_{Tjk}}{\partial x_{Tjk}} = \begin{bmatrix} i_{jk}^T & v_{jk}^T & i_{kj}^T \end{bmatrix}^T$, $R_{Tjk} = \text{diag}\left(r_{jk}I, \frac{1}{r_\infty}I, r_{kj}I\right) > 0$, $G_{jk} = \begin{bmatrix} I & 0 & 0 \end{bmatrix}$, $G_{kj} = \begin{bmatrix} 0 & 0 & I \end{bmatrix}$ and

$$J_{Tjk} = \begin{bmatrix} 0 & -I & 0 \\ I & 0 & I \\ 0 & -I & 0 \end{bmatrix}.$$

3) Modeling of π-type T&D Lines: A π-type T&D line is illustrated as shown in Figure 6.

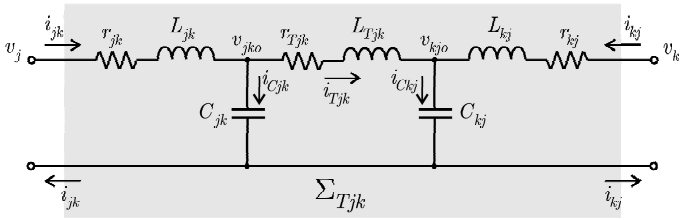

Figure 6. A π-type T&D line between the nodes j and k.

Similarly, according to the KCL/KVL, there are

$$\begin{aligned} L_{jk}\frac{di_{jk}}{dt} &= -r_{jk}i_{jk} - v_{jko} + v_j \\ C_{jk}\frac{dv_{jko}}{dt} &= i_{jk} - i_{Tjk} - \frac{1}{r_\infty}v_{jko} \\ L_{kj}\frac{di_{kj}}{dt} &= -r_{kj}i_{kj} - v_{kjo} + v_k \\ C_{kj}\frac{dv_{kjo}}{dt} &= i_{kj} + i_{Tjk} - \frac{1}{r_\infty}v_{kjo} \\ L_{Tjk}\frac{di_{Tjk}}{dt} &= -r_{Tjk}i_{Tjk} - v_{kjo} + v_{jko}, \end{aligned} \tag{15}$$

where r_∞ denotes the large resistor in parallel with the capacitors (not shown in the figure). The actual resistor value for each capacitor may be different but it is fine to use the same notation in the model. By selecting the state vector as

$$x_{Tjk} = \begin{bmatrix} L_{jk}i_{jk}^T & C_{jk}v_{jko}^T & L_{kj}i_{kj}^T & C_{kj}v_{kjo}^T & L_{Tjk}i_{Tjk}^T \end{bmatrix}^T, \tag{16}$$

and the Hamiltonian function as

$$\begin{aligned} H_T = &\frac{1}{2}L_{jk}i_{jk}^T i_{jk} + \frac{1}{2}C_{jk}v_{jko}^T v_{jko} \\ &+ \frac{1}{2}L_{kj}i_{kj}^T i_{kj} + \frac{1}{2}C_{kj}v_{kjo}^T v_{kjo} + \frac{1}{2}L_{Tjk}i_{Tjk}^T i_{Tjk}, \end{aligned} \tag{17}$$

the π-type T&D line (15) shown in Figure 6 can be expressed in the format (8) as well

with $\frac{\partial H_{Tjk}}{\partial x_{Tjk}} = \begin{bmatrix} i_{jk}^T & v_{jko}^T & i_{kj}^T & v_{kjo}^T & i_{Tjk}^T \end{bmatrix}^T$, $R_{Tjk} = \text{diag}\left(r_{jk}I,\, \frac{1}{r_\infty}I,\, r_{kj}I,\, \frac{1}{r_\infty}I,\, r_{Tjk}I\right) > 0$, $G_{jk} = \begin{bmatrix} I & 0 & 0 & 0 & 0 \end{bmatrix}$, $G_{kj} = \begin{bmatrix} 0 & 0 & I & 0 & 0 \end{bmatrix}$, and $J_{Tjk} = \begin{bmatrix} 0 & -I & 0 & 0 & 0 \\ I & 0 & 0 & 0 & -I \\ 0 & 0 & 0 & -I & 0 \\ 0 & 0 & I & 0 & I \\ 0 & I & 0 & -I & 0 \end{bmatrix}$.

B. Modeling of a Generic Passive Power Grid

Figure 2 illustrates a generic meshed power grid $\hat{\Sigma}$ with N nodes linked through a passive T&D grid with M T&D lines. The T&D lines can be of different types. However, since their models are in the same format as described in (8) with different matrices, it is possible to establish the model of the power grid by stacking up the models of different T&D lines.

With the models of the M T&D lines in the format of (8) with matrices of appropriate dimensions, the model Σ_G for the power grid in Figure 2 with N nodes and M T&D lines can be obtained as

$$\Sigma_G : \begin{cases} \dot{x}_G = (J_G - R_G)\dfrac{\partial H_G}{\partial x_G} + G_G^T B^T \begin{bmatrix} v_1 \\ \vdots \\ v_N \end{bmatrix} \\ \begin{bmatrix} i_{o1} \\ \vdots \\ i_{oN} \end{bmatrix} = BG_G\dfrac{\partial H_G}{\partial x_G} = \begin{bmatrix} B_1 \\ \vdots \\ B_N \end{bmatrix} G_G \dfrac{\partial H_G}{\partial x_G}, \end{cases} \tag{18}$$

where i_{ol} represents the current injected into the T&D grid at the lth node ($l \in \mathcal{N}$); v_l represents the voltage of the lth node ($l \in \mathcal{N}$); $B \triangleq \begin{bmatrix} B_1^T & \dots & B_N^T \end{bmatrix}^T \in \{0, I\}^{(3N)\times(3nM)}$ represents the connection of the M T&D lines with the N nodes (with I representing being connected and 0 being not connected); the state vector $x_G \in \mathbb{R}^{3nM\times 1}$ represents the states of the M T&D lines stacked together; $G_G = \text{diag}_m\left(\begin{bmatrix} G_{jk} \\ G_{kj} \end{bmatrix}\right)$, $j, k \in \mathcal{N} \setminus \{j = k\}$ represents the output matrices of the T&D lines stacked together; $J_G = -J_G^T = \text{diag}_m(J_{Tjk}) \in \mathbb{R}^{3nM\times 3nM}$ and $R_G = R_G^T = \text{diag}_m(R_{Tjk}) > 0 \in \mathbb{R}^{3nM\times 3nM}$ represents the state matrices of the T&D lines stacked together; and the non-negative function $H_G(x_G) = \Sigma_m H_{Tjk} : \mathbb{R}^{3nM} \to [0, \infty)$ represents the total energy function of the T&D grid (lines). Here, the subscript $_m$ indicates the operation over all T&D lines ($1 \le m \le M$). Since $i_{jk}, i_{kj} \subseteq G_G\dfrac{\partial H_G}{\partial x_G}$, $j, k \in \mathcal{N}\setminus\{j = k\}$, the matrix B_l ($l \in \mathcal{N}$) selects the line currents i_{jk} and i_{kj} flowing into the T&D lines to yield the current i_{ol} for the Node l. The number of non-zero blocks I in each column of the B matrix is 1, indicating that each end of a T&D line can only be connected to one node. The number of non-zero blocks I in B_l ($l \in \mathcal{N}$) is equal to the number of the T&D lines connected to the Node l. Note that the non-zero blocks I in B^T indicate the corresponding T&D line terminal voltage associated. In other words, the matrix B can be regarded as the mapping from the T&D line currents $i_T = G_G\dfrac{\partial H_G}{\partial x_G}$ to the currents flowing into the nodes i_{ol}, $l \in \mathcal{N}$, while the matrix B^T associates the node voltages to the T&D lines.

Since every T&D line has its interconnection matrix $J_{Tjk} = -J_{Tjk}^T$ and damping matrix $R_{Tjk} > 0$, the same follows for J_G and R_G. As a result, the T&D grid Σ_G is passive.

Example 2. In order to illustrate the stack-up of the model, the power grid shown in Figure 7 is given below as an example. Assume the π-type T&D lines are adopted for this power grid. There are $N = 4$ nodes and $M = 5$ T&D lines. The node current vector is $i_o = \begin{bmatrix} i_{o1}^T & i_{o2}^T & i_{o3}^T & i_{o4}^T \end{bmatrix}^T$ and the node voltage vector is $\begin{bmatrix} v_1^T & v_2^T & v_3^T & v_4^T \end{bmatrix}^T$. Each T&D line is modeled with H_{Tjk}, $(j,k) \in \mathcal{E} = \{(1,2),(1,4),(2,3),(2,4),(3,4)\}$, with $\frac{\partial H_{Tjk}}{\partial x_{Tjk}} = \begin{bmatrix} i_{jk}^T & v_{jko}^T & i_{kj}^T & v_{kjo}^T & i_{Tjk}^T \end{bmatrix}^T$, as discussed in Section III-A3. As a result, the total energy function of the grid is $H_G = H_{T12} + H_{T14} + H_{T23} + H_{T24} + H_{T34}$ and the state of the grid is $x_G = \begin{bmatrix} x_{T12}^T & x_{T14}^T & x_{T23}^T & x_{T24}^T & x_{T34}^T \end{bmatrix}^T$, which implies $\frac{\partial H_G}{\partial x_G} = \left[\left(\frac{\partial H_{T12}}{\partial x_{T12}}\right)^T \left(\frac{\partial H_{T14}}{\partial x_{T14}}\right)^T \left(\frac{\partial H_{T23}}{\partial x_{T23}}\right)^T \left(\frac{\partial H_{T24}}{\partial x_{T24}}\right)^T \left(\frac{\partial H_{T34}}{\partial x_{T34}}\right)^T\right]^T$ for the model (18) with the T&D line currents stacked together in the order of the T&D lines as $i_T = \begin{bmatrix} i_{12}^T & i_{21}^T & i_{14}^T & i_{41}^T & i_{23}^T & i_{32}^T & i_{24}^T & i_{42}^T & i_{34}^T & i_{43}^T \end{bmatrix}^T$, $J_G = -J_G^T = \text{diag}(J_{T12}, J_{T14}, J_{T23}, J_{T24}, J_{T34})$, $R_G = R_G^T = \text{diag}(R_{T12}, R_{T14}, R_{T23}, R_{T24}, R_{T34}) > 0$,

$$G_G = \text{diag}\left(\begin{bmatrix} G_{12} \\ G_{21} \end{bmatrix}, \begin{bmatrix} G_{14} \\ G_{41} \end{bmatrix}, \begin{bmatrix} G_{23} \\ G_{32} \end{bmatrix}, \begin{bmatrix} G_{24} \\ G_{42} \end{bmatrix}, \begin{bmatrix} G_{34} \\ G_{43} \end{bmatrix}\right),$$

and

$$B = \begin{bmatrix} B_1 \\ B_2 \\ B_3 \\ B_4 \end{bmatrix} = \begin{bmatrix} I & 0 & I & 0 & 0 & 0 & 0 & 0 & 0 & 0 \\ 0 & I & 0 & 0 & I & 0 & I & 0 & 0 & 0 \\ 0 & 0 & 0 & 0 & 0 & I & 0 & 0 & I & 0 \\ 0 & 0 & 0 & I & 0 & 0 & 0 & I & 0 & I \end{bmatrix} \tag{19}$$

that maps the T&D line currents i_T to the node current vector i_o, i.e., $i_o = Bi_T$.

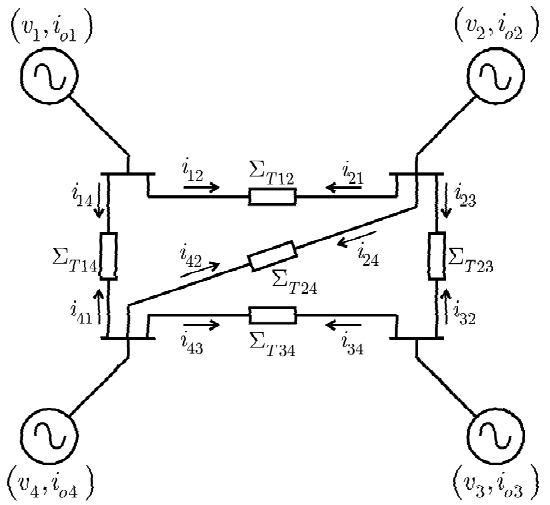

Figure 7. An example power grid with $N = 4$ nodes and $M = 5$ T&D lines, which will be used as the testbed and studied further in Section VI.

IV. Modeling and Control of Power Converters

A. Modeling of a DC/AC Power Converter

The model of the power grid formed by passive T&D lines in a meshed configuration is given by (18). At the nodes,

power converters or generators can be connected. In this paper, it is assumed that DC/AC power electronic converters are connected at the nodes. Note that, strictly speaking, neither a power converter nor a generator "generates" electricity because it only converts one type of energy to electricity.

Figure 8 illustrates a DC/AC power converter with a local load. Again, without loss of generality, a three-phase system is considered but the development can be easily adapted to single-phase systems as well. Ideal voltage sources e are adopted to model DC/AC power converters that in practice are pulse-width modulated with a frequency high enough so that the switching dynamics can be neglected. Furthermore, in practice, the effects of fluctuations on the DC side voltage can be compensated in the pulse width modulation and hence are omitted as well.

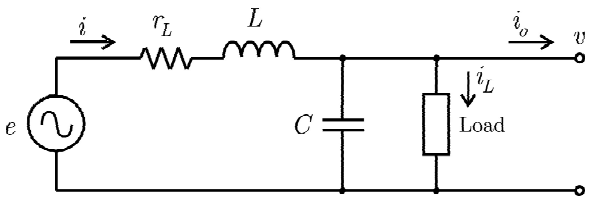

Figure 8. Equivalent model of a DC/AC power converter with a local load.

The local loads can be linear and switched nonlinear loads, such as voltage controlled rectifiers, which can be modeled in the general pH format as [22]

$$\Sigma_L: \begin{cases} M_L\dot{q} = [J_L(q,d) - R_L]\dfrac{\partial H_L}{\partial q} + G_L^T v \\ i_L = G_L\dfrac{\partial H_L}{\partial q}, \end{cases} \tag{20}$$

with the load input voltage v, the output load current i_L and matrices $J_L = -J_L^T$ and $R_L = R_L^T > 0$. The state vector is $q \in \mathbb{R}^{n_L}$, where n_L depends on the dynamics of the load, the Hamiltonian is $H_L = \frac{1}{2}q^T M_L q : \mathbb{R}^{n_L} \to [0, \infty)$, with $M_L = \mathrm{diag}(m_1, \ldots, m_{n_L}) > 0$. The vector d is used to model the (bounded) modulation index in the case of switched power electronic loads.

Applying the KCL/KVL to the LC filter in Figure 8 while considering a large resistor r_∞ in parallel with the capacitor not shown in the figure, there are

$$\begin{aligned} L\frac{di}{dt} &= -r_L i - v + e \\ C\frac{dv}{dt} &= i - i_L - i_o - \frac{1}{r_\infty}v. \end{aligned}$$

Together with the load model (20), the model of the system Σ_P comprising the power converter and the local passive load can be derived as

$$\Sigma_P: \begin{cases} \dot{x}_P = [J_P(x_P) - R_P]\dfrac{\partial H_P(x_P)}{\partial x_P} + G_P^T e + G_{oP}^T i_o \\ i = G_P\dfrac{\partial H_P(x_P)}{\partial x_P} \\ -v = G_{oP}\dfrac{\partial H_P(x_P)}{\partial x_P}, \end{cases} \tag{21}$$

with $e = \begin{bmatrix} e_a & e_b & e_c \end{bmatrix}^T$, $x_P = \begin{bmatrix} Li^T & Cv^T & M_L q^T \end{bmatrix}^T$, $i_o = \begin{bmatrix} i_{oa} & i_{ob} & i_{oc} \end{bmatrix}^T$, the Hamiltonian

$$H_P = \frac{1}{2}Li^T i + \frac{1}{2}Cv^T v + \frac{1}{2}q^T M_L q, \tag{22}$$

$G_P = \begin{bmatrix} I & 0 & 0 \end{bmatrix}$, $G_{oP} = \begin{bmatrix} 0 & -I & 0 \end{bmatrix}$, $R_P = \mathrm{diag}\left(r_L I,\ \frac{1}{r_\infty}I,\ R_L I\right) > 0$ and

$$J_P(x_P) = \begin{bmatrix} 0 & -I & 0 \\ I & 0 & -G_L \\ 0 & G_L^T & J_L(q,d) \end{bmatrix}.$$

The system (21) has two passive power ports, (e, i) and $(i_o, -v)$, which can be used for connecting the power converter with the controller and the environment, respectively.

B. Generic Control Framework for a DC/AC Power Converter

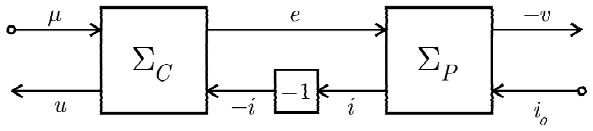

Figure 9. A generic control framework to achieve passivity for a power converter.

Instead of proposing a particular controller, a general control framework is proposed here to render the closed-loop power converter passive. The control framework is shown in Figure 9 with a generic passive controller Σ_C given by

$$\Sigma_C: \begin{cases} \dot{x}_C = (J_C(x_C) - R_C(x_C))\dfrac{\partial H_C}{\partial x_C} + G_C^T(-i) + G_{\mu C}^T\mu \\ e = G_C\dfrac{\partial H_C}{\partial x_C} \\ u = G_{\mu C}\dfrac{\partial H_C}{\partial x_C}, \end{cases} \tag{23}$$

with $J_C(x_C) = -J_C^T(x_C)$, $R_C(x_C) = R_C^T(x_C) > 0$, the controller Hamiltonian $H_C = \frac{1}{2}x_C^T M_C x_C : \mathbb{R}^{\dim x_C} \to [0, \infty)$, the controller state x_C, and the exogenous reference input μ. The output u may be the same as the output voltage e but can be different. Accordingly, $\dim\mu = \dim u$ and can be designed to be equal to dim$e$ or not, depending on the input matrix $G_{\mu C}^T$. The reference input μ could contain suitable combination of the desired system frequency, voltage, real power, reactive power, etc. The $(e, -i)$ port of the passive controller Σ_C described in (23) is interconnected with the (e, i) port of the power converter Σ_P described in (21) through the negative feedback of i. That is to connect the output e of the controller Σ_C to the input e of the plant Σ_P and the output i of the plant Σ_P to the input $-i$ of the controller Σ_C through the negative feedback of i. Note that the state matrices can be state dependent.

Remark 3. Such a controller can be found in [19].

The following result describes an important property of the control framework.

Lemma 4. *The closed-loop control system of Figure 9 with the power converter modeled by (21) and the controller given in (23) is passive. Moreover, it is ISS when operated independently, i.e., when $i_o = 0$.*

Proof: Define the state vector of the controlled converter as $x = \begin{bmatrix} x_P^T & x_C^T \end{bmatrix}^T$ and its Hamiltonian as $H(x) = H_P(x_P) + H_C(x_C)$. The closed-loop system shown in Figure 9 can then be modeled, via stacking up the state equations in (23) and (21) and substituting the interconnected signals with $i = G_P \frac{\partial H_P(x_P)}{\partial x_P}$ and $e = G_C \frac{\partial H_C}{\partial x_C}$, as

$$\Sigma: \begin{cases} \dot{x} = [J(x) - R(x)] \dfrac{\partial H(x)}{\partial x} + G_o^T i_o + G_\mu^T \mu \\ -v = G_o \dfrac{\partial H(x)}{\partial x} \\ u = G_\mu \dfrac{\partial H(x)}{\partial x}, \end{cases} \tag{24}$$

with $R = \text{diag}(R_P, R_C) > 0$, $G_o = \begin{bmatrix} G_{oP} & 0 \end{bmatrix}$, $G_\mu = \begin{bmatrix} 0 & G_{\mu C} \end{bmatrix}$, and the skew symmetric matrix

$$J = \begin{bmatrix} J_P & G_P^T G_C \\ -G_C^T G_P & J_C \end{bmatrix}.$$

Because the power converter modeled in (21) and the controller given in (23) are both passive, the closed-loop system as modeled in (24) is passive as well. By letting $i_o = 0$, it is clear that the closed-loop system is ISS because the reference input μ is bounded, according to Lemma 1. ■

V. Compact Model and Input-to-State Stability of Generic Power Systems

A. Compact Model of Generic Power Systems

The generic power system shown in Figure 2 with N power converters Σ_l ($l \in \mathcal{N}$) connected at the nodes, which are interconnected through a generic passive T&D grid, can be modeled as shown in Figure 10, via interconnecting the $(-v_l, i_{ol})$ port of the closed-loop passive power converter Σ_l with the (v_l, i_{ol}) port of the T&D grid Σ_G through the negative feedback of voltage $-v_l$. That is to connect the output $-v_l$ of the closed-loop passive power converter Σ_l to the input v_l of the T&D grid Σ_G through the negative feedback of voltage $-v_l$ and to connect the output i_{ol} of the T&D grid Σ_G to the input i_{ol} of the closed-loop passive power converter Σ_l. This reveals an important negative-feedback feature between the power converters and the grid, which is critical in maintaining the stability of power systems.

Denote the lth power converter connected to the lth node of the power grid Σ_G as Σ_l ($l \in \mathcal{N}$), according to (24), with H_l being its Hamiltonian and x_l being its state vector. Furthermore, define the state vector of the power system $\hat{\Sigma}$ by stacking up the state vectors of the closed-loop power converters Σ_l and the T&D grid Σ_G as $\hat{x} = \begin{bmatrix} x_1^T & \dots & x_N^T & x_G^T \end{bmatrix}^T$ with the system Hamiltonian $\hat{H} = \Sigma_{l=1}^N H_l + H_G$. Stacking up the state equations of the N converters and the grid Σ_G, there is

$$\begin{bmatrix} \dot{x}_1 \\ \vdots \\ x_N \\ x_G \end{bmatrix} = \begin{bmatrix} J_1(x_1) - R_1(x_1) & \cdots & 0 & 0 \\ \vdots & \ddots & \vdots & \vdots \\ 0 & \cdots & J_N(x_N) - R_N(x_N) & 0 \\ 0 & \dots & 0 & J_G - R_G \end{bmatrix} \begin{bmatrix} \dfrac{\partial H_1(x_1)}{\partial x_1} \\ \vdots \\ \dfrac{\partial H_N(x_N)}{\partial x_N} \\ \dfrac{\partial H_G(x_G)}{\partial x_G} \end{bmatrix} + \begin{bmatrix} G_{o1}^T & \cdots & 0 \\ \vdots & \ddots & \vdots \\ 0 & \cdots & G_{oN}^T \\ 0 & \dots & 0 \end{bmatrix} \begin{bmatrix} i_{o1} \\ \vdots \\ i_{oN} \end{bmatrix}$$
$$+ \begin{bmatrix} G_{\mu 1}^T(x_1) & \cdots & 0 \\ \vdots & \ddots & \vdots \\ 0 & \cdots & G_{\mu N}^T(x_N) \\ 0 & \dots & 0 \end{bmatrix} \begin{bmatrix} \mu_1 \\ \vdots \\ \mu_N \end{bmatrix} + \begin{bmatrix} 0 & \cdots & 0 \\ \vdots & \ddots & \vdots \\ 0 & \cdots & 0 \\ G_G^T B^T \end{bmatrix} \begin{bmatrix} v_1 \\ \vdots \\ v_N \end{bmatrix}. \tag{25}$$

Then, by replacing the node voltage vector $\begin{bmatrix} v_1^T & \dots & v_N^T \end{bmatrix}^T$ with $\left[-\left(G_{o1} \frac{\partial H_1}{\partial x_1} \right)^T \quad \dots \quad -\left(G_{oN} \frac{\partial H_N}{\partial x_N} \right)^T \right]^T$ and the node current vector $\begin{bmatrix} i_{o1}^T & \dots & i_{oN}^T \end{bmatrix}^T$ with $BG_G \frac{\partial H_G}{\partial x_G}$, respectively, according to (24) and (18), while noting $B = \begin{bmatrix} B_1^T & \dots & B_N^T \end{bmatrix}^T$,

the power system $\hat{\Sigma}$ can be described as

$$\hat{\Sigma}: \begin{cases} \begin{bmatrix} \dot{x}_1 \\ \vdots \\ x_N \\ x_G \end{bmatrix} = \begin{bmatrix} J_1(x_1) - R_1(x_1) & \cdots & 0 & G_{o1}^T B_1 G_G \\ \vdots & \ddots & \vdots & \vdots \\ 0 & \cdots & J_N(x_N) - R_N(x_N) & G_{oN}^T B_N G_G \\ -G_G^T B_1^T G_{o1} & \cdots & -G_G^T B_N^T G_{oN} & J_G - R_G \end{bmatrix} \begin{bmatrix} \frac{\partial \hat{H}}{\partial x_1} \\ \vdots \\ \frac{\partial \hat{H}}{\partial x_N} \\ \frac{\partial \hat{H}}{\partial x_G} \end{bmatrix} + \begin{bmatrix} G_{\mu 1}^T(x_1) & \cdots & 0 \\ \vdots & \ddots & \vdots \\ 0 & \cdots & G_{\mu N}^T(x_N) \\ 0 & \dots & 0 \end{bmatrix} \begin{bmatrix} \mu_1 \\ \vdots \\ \mu_N \end{bmatrix} \\ \begin{bmatrix} u_1 \\ \vdots \\ u_N \end{bmatrix} = \begin{bmatrix} G_{\mu 1}(x_1) & \cdots & 0 & 0 \\ \vdots & \ddots & \vdots & \vdots \\ 0 & \cdots & G_{\mu N}(x_N) & 0 \end{bmatrix} \begin{bmatrix} \frac{\partial \hat{H}}{\partial x_1} \\ \vdots \\ \frac{\partial \hat{H}}{\partial x_N} \\ \frac{\partial \hat{H}}{\partial x_G} \end{bmatrix}, \end{cases} \tag{26}$$

because $\dfrac{\partial \hat{H}}{\partial x_G} = \dfrac{\partial H_G}{\partial x_G}$ and $\dfrac{\partial \hat{H}}{\partial x_l} = \dfrac{\partial H_l}{\partial x_l}$ $(l \in \mathcal{N})$.

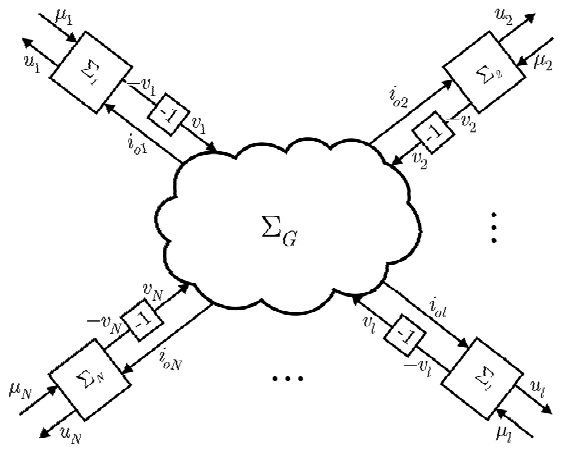

Figure 10. Model of the generic power system $\hat{\Sigma}$ in Figure 2 with N power converters Σ_l $(l \in \mathcal{N})$ connected at the nodes, which are interconnected through a generic passive grid Σ_G.

This compact formula has established the complete mathematical model for a generic power system consisting of local loads and multiple power converters that are controlled with generic passive controllers and interconnected through a passive T&D grid. It is expected to play a foundational role in future research and implementation of power systems dominated by power electronic converters. To the best knowledge of the authors, such a generic compact model and control framework that covers the whole power system has not been developed in the literature.

B. Input-to-State Stability of Generic Power Systems

The following result shows that the resulting system is ISS.

Theorem 5. *As described by the compact mathematical model (26) and illustrated in Figure 10, the power system shown in Figure 2 with power converters connected at the nodes, which are interconnected through generic passive T&D lines in a meshed configuration, is passive and ISS if all the power converters with local passive loads as described in (20) are controlled in the generic framework shown in Figure 9 with a passive controller given in (23).*

Proof: From the passivity of Σ_G and Σ_l, $l \in \mathcal{N}$, it is clear that the power system $\hat{\Sigma}$ shown in (26) is passive. Moreover, the power system $\hat{\Sigma}$ in (26) satisfies the conditions in Lemma 1 and the references μ_l are bounded. As a result, it is ISS. ■

Note that the matrix $B = \begin{bmatrix} B_1^T & \dots & B_N^T \end{bmatrix}^T$, which represents the topology of the T&D grid, only appears in the skew-symmetric matrix of the system (26). As a result, the grid topology does not affect the upper bound γ described in (7), although it affects the system dynamics.

Remark 6. The result of Theorem 5 is generic and valid whenever the power converters are controlled according the controller of Section IV-B, irrespective of their parameters.

VI. Case Study

A. Description of the System

Computational simulations are carried out with the 4-converter three-phase power system, as shown in Figure 7, which is discussed in Example 2. The lengths of the T&D lines Σ_{T12}, Σ_{T14}, Σ_{T23}, Σ_{T24} and Σ_{T34} are 15 km, 12 km, 10 km, 25 km and 8 km, respectively, and the T&D lines are assumed to be of π-type as shown in Figure 6 but with the RL branches at both ends neglected because of the relatively short line lengths. The lumped model parameters are $0.0127\,\Omega/\mathrm{km}$, $0.934\,\mathrm{mH/km}$ and $12.740\,\mathrm{nF/km}$, respectively. The system line-line voltage is 480V, i.e., with a phase voltage of $V_n = 277$ V (rms), and the system frequency is 60 Hz. The inverters are rated at 50 kVA, 100 kVA, 150kVA and 25 kVA, respectively. The inverters are controlled by the controller introduced in [19], which meets the requirements given in Section IV-B.

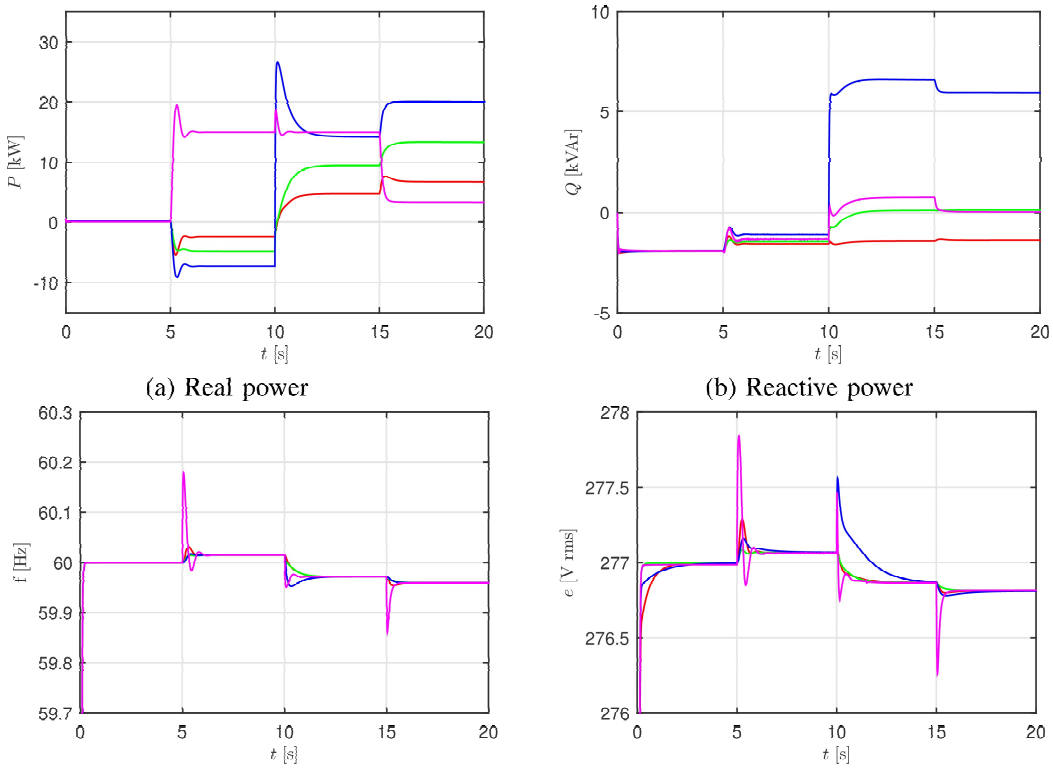

(a) Real power (b) Reactive power

(c) Frequency (d) RMS voltages

Figure 11. Simulation results from the system shown in Figure 7 (curves in red, green, blue and magenta representing Converters 1, 2, 3 and 4, respectively).

The voltage synthesized by the power converters are given by $e = \omega\varphi\psi \left[\sin\omega t \quad \sin\left(\omega t - \frac{2\pi}{3}\right) \quad \sin\left(\omega t + \frac{2\pi}{3}\right)\right]^T$, where ω is the frequency and φ and ψ are state variables that are introduced to yield a passive controller. All power converters have the same droop coefficients, which are 0.5% for the frequency and 5% for φ and ψ. Note that the controller design does not need the converter parameters, such as the LC filters. For information only, the filter capacitors are 22 μF while the filter inductors are 1.5 mH.

B. Simulation Results

The real and reactive powers, RMS voltages and frequencies of the converters are given in Figure 11, corresponding to the simulations carried out in the following sequence:

- At $t = 0$ s, all four power converters are started to operate in the droop mode. Quickly, the frequencies settle down at 60Hz and the voltages settle down at 277V.
- At $t = 5$ s, Converter 4 operates in the set mode with a real-power reference of 15 kW. It tracks the reference well while the other converters absorb the real power according to their power ratings. In addition, the voltages and frequencies of the inverters settle down quickly. Some oscillations are observed in the reactive power because no low-pass filter is used.
- At $t = 10$ s, a constant power load of 45 kW and 5 kVAr (inductive) is connected at the terminals of Converter 3, with Converter 4 still injecting 15 kW. The other three converters share the remaining 30 kW load proportionally according their power ratings.
- At $t = 15$ s, Converter 4 operates in the droop mode after removing the 15kW real-power reference. As a consequence, the load is supplied by all the power converters according to their power ratings.

The voltages and frequencies of all inverters are maintained within the desired ranges of +/-5% and +/-0.5%, respectively, during the whole process. Due to different line lengths and system parameters, the reactive powers of the converters are not shared proportionally to their power ratings, but the voltages at the terminals are regulated well.

VII. Conclusions

In this paper, a generic control framework with a passive controller has been proposed for DC/AC power converters. Moreover, a complete compact mathematical model has been developed for generic power systems dominated by DC/AC power converters, which are controlled by the proposed control framework and interconnected through a generic T&D grid without self-loops in meshed configurations. The model of generic T&D lines has also been developed, which is applicable to different types of T&D lines. It has been proven that the DC/AC power converters with the proposed control framework are passive and ISS when operated independently or collectively in a power system. Furthermore, no assumptions on constant frequency/voltage or lossless grid are made. The analysis is made for balanced three-phase systems in order to simplify the presentation but can be adapted for single-phase and unbalanced three-phase systems easily because no particular tools are adopted. The power grid is modeled to reveal power

ports that allow the connection of voltage-source converters at the nodes. The extension to current-source converters is under investigation. Another topic under investigation is to include conventional players, such as synchronous generators, in the model. Furthermore, studies are being made to finally prove the asymptotic stability of future power systems, including the one based on the SYNDEM grid architecture, which homogenizes and harmonizes heterogeneous power systems players with the VSM technology.

REFERENCES

[1] Q.-C. Zhong, *Power Electronics-Enabled Autonomous Power Systems: Next Generation Smart Grids*. Wiley-IEEE Press, 2020.

[2] Q.-C. Zhong and T. Hornik, *Control of Power Inverters in Renewable Energy and Smart Grid Integration*. Wiley-IEEE Press, 2013.

[3] J. Carrasco, L. Franquelo, J. Bialasiewicz, E. Galvan, R. Portillo-Guisado, M. Prats, J. Leon, and N. Moreno-Alfonso, "Power-electronic systems for the grid integration of renewable energy sources: A survey," *IEEE Trans. Ind. Electron.*, vol. 53, no. 4, pp. 1002–1016, Jun. 2006.

[4] Q.-C. Zhong, "Virtual synchronous machines: A unified interface for smart grid integration," *IEEE Power Electronics Magazine*, vol. 3, no. 4, pp. 18–27, Dec 2016.

[5] S. Fiaz, D. Zonetti, R. Ortega, J. M. A. Scherpen, and A. J. Van der Schaft, "A port-Hamiltonian approach to power network modeling and analysis," *European Journal of Control*, vol. 19, no. 6, pp. 477–485, 2013.

[6] D. Groß, M. Colombino, J.-S. Brouillon, and F. Dörfler, "The effect of transmission-line dynamics on grid-forming dispatchable virtual oscillator control," *IEEE Transactions on Control of Network Systems*, vol. 6, no. 3, pp. 1148–1160, 2019.

[7] Y. Guo, D. Zhang, Z. Li, Q. Wang, and D. Yu, "Overviews on the applications of the kuramoto model in modern power system analysis," *International Journal of Electrical Power & Energy Systems*, vol. 129, p. 106804, 2021. [Online]. Available: https://www.sciencedirect.com/science/article/pii/S0142061521000442

[8] J. W. Simpson-Porco, F. Dörfler, and F. Bullo, "Droop-controlled inverters are kuramoto oscillators," *IFAC Proceedings Volumes*, vol. 45, no. 26, pp. 264–269, 2012.

[9] J. Schiffer, R. Ortega, A. Astolfi, J. Raisch, and T. Sezi, "Conditions for stability of droop-controlled inverter-based microgrids," *Automatica*, vol. 50, no. 10, pp. 2457–2469, 2014.

[10] J. Schiffer, E. Fridman, R. Ortega, and J. Raisch, "Stability of a class of delayed port-hamiltonian systems with application to microgrids with distributed rotational and electronic generation," *Automatica*, vol. 74, pp. 71–79, 2016.

[11] D. Pan, X. Wang, F. Liu, and R. Shi, "Transient stability of voltage-source converters with grid-forming control: A design-oriented study," *IEEE Journal of Emerging and Selected Topics in Power Electronics*, vol. 8, no. 2, pp. 1019–1033, jun 2020.

[12] I. Subotic, D. Gros, M. Colombino, and F. Dorfler, "A lyapunov framework for nested dynamical systems on multiple time scales with application to converter-based power systems," *IEEE Transactions on Automatic Control*, vol. 66, no. 12, pp. 5909–5924, dec 2021.

[13] K. D. Smith, S. Jafarpour, and F. Bullo, "Transient stability of droop-controlled inverter networks with operating constraints," *IEEE Transactions on Automatic Control*, vol. 67, no. 2, pp. 633–645, feb 2022.

[14] A. van der Schaft and D. Jeltsema, "Port-Hamiltonian systems theory: An introductory overview," *Foundations and Trends in Systems and Control*, vol. 1, no. 2-3, pp. 173–378, 2014. [Online]. Available: http://dx.doi.org/10.1561/2600000002

[15] B. Maschke and A. Van Der Schaft, "Port controlled Hamiltonian systems: modeling origins and system theoretic properties," in *IFAC Symp. Nonlinear Control Systems Design*, 1991, pp. 359–365.

[16] R. Ortega, A. J. van der Schaft, I. Mareels, and B. Maschke, "Putting energy back in control," *IEEE Control Systems*, vol. 21, no. 2, pp. 18–33, 2001.

[17] R. Ortega, A. van der Schaft, F. Castanos, and A. Astolfi, "Control by interconnection and standard passivity-based control of port-Hamiltonian systems," *IEEE Transactions on Automatic Control*, vol. 53, no. 11, pp. 2527–2542, Dec. 2008.

[18] S. Avila-Becerril, G. Espinosa-Pérez, and J. E. Machado, "A hamiltonian control approach for electric microgrids with dynamic power flow solution," *Automatica*, vol. 139, p. 110192, 2022. [Online]. Available: https://www.sciencedirect.com/science/article/pii/S0005109822000371

[19] Q.-C. Zhong and M. Stefanello, "A port-hamiltonian control framework to render a power electronic system passive," *IEEE Transactions on Automatic Control*, vol. 67, no. 4, pp. 1960–1965, 2022.

[20] A. van der Schaft, "L2 - gain and passivity techniques in nonlinear control," 2000.

[21] G. C. Konstantopoulos, Q.-C. Zhong, B. Ren, and M. Krstic, "Stability analysis and fail-safe operation of inverters operated in parallel," *International Journal of Control*, vol. 88, no. 7, pp. 1410–1421, 2015.

[22] G. C. Konstantopoulos and A. T. Alexandridis, "Generalized nonlinear stabilizing controllers for Hamiltonian-passive systems with switching devices," *IEEE Trans. Control Syst. Technol.*, vol. 21, no. 4, pp. 1479–1488, 2013.

Qing-Chang Zhong (M'04-SM'04-F'17) received the Ph.D. degree in control and power engineering from Imperial College London in 2004 and the Ph.D. degree in control theory and engineering from Shanghai Jiao Tong University in 2000.

He holds the Max McGraw Endowed Chair Professor in Energy and Power Engineering at Dept. of Electrical and Computer Engineering, Illinois Institute of Technology, and is the Founder and CEO of Syndem LLC, Chicago, USA. He served as a Steering Committee member for IEEE Smart Grid, a Distinguished Lecturer for IEEE PELS/CSS/PES/IES Societies, an Associate Editor for IEEE TAC/TIE/TPELS/TCST/Access/JESTPE, and a Vice-Chair for IFAC TC Power and Energy Systems. He proposed the synchronized and democratized (SYNDEM) smart grid architecture to unify the integration of non-synchronous distributed energy resources and flexible loads with the synchronization mechanism of synchronous machines. He authored four research monographs, including *Power Electronics-enabled Autonomous Power Systems: Next Generation Smart Grids* (Wiley-IEEE Press, 2020) and *Control of Power Inverters in Renewable Energy and Smart Grid Integration* (Wiley-IEEE Press, 2013). He currently chairs the Working Group of IEEE Standard on Virtual Synchronous Machines.

Márcio Stefanello (M'07) received the M.Sc. and Ph.D. degrees in electrical engineering from the Federal University of Santa Maria, Santa Maria, Brazil, in 2006 and 2010, respectively. Since 2010, he has been with the Federal University of Pampa (UNIPAMPA), Alegrete, Brazil, as a professor and is the head of the Laboratory of Energy Processing and Control (LaPEC). From 2016 to 2017 he was with the Department of Electrical and Computer Engineering, Illinois Institute of Technology, Chicago, USA, as a visiting scholar. His current research interests include adaptive control, control of grid-connected converters, and microgrids. Dr. Stefanello is a member of IEEE.